



JGR Space Physics

RESEARCH ARTICLE

10.1029/2023JA032353

Key Points:

- Most lightning-generated whistlers exhibit oblique and outward wave normal angles in the region of L < 3
- In the very low altitude (<0.2R_E)
 region, oblique and inward propagation
 modes of LGWs exist
- A ray tracing simulation confirms the dominant outward propagation and the existence of inward propagation

Supporting Information:

Supporting Information may be found in the online version of this article.

Correspondence to:

Z. Xia, Zhiyang.Xia@utdallas.edu

Citation:

Xia, Z., Chen, L., Horne, R. B., Liu, X., He, J., & Bortnik, J. (2024). On the wavenormal distribution of lightning-generated whistlers and their propagation modes. *Journal of Geophysical Research: Space Physics*, 129, e2023JA032353. https://doi.org/10.1029/2023JA032353

Received 7 DEC 2023 Accepted 10 MAR 2024

On the Wave-Normal Distribution of Lightning-Generated Whistlers and Their Propagation Modes

Zhiyang Xia¹, Lunjin Chen¹, Richard B. Horne², Xu Liu¹, Jiabei He¹, and Jacob Bortnik³

¹Department of Physics, University of Texas at Dallas, Richardson, TX, USA, ²British Antarctic Survey, Cambridge, UK, ³Department of Atmospheric and Oceanic Sciences, UCLA, Los Angeles, CA, USA

Abstract Observations from Van Allen Probes are analyzed to obtain the statistical wave normal distribution of lightning-generated whistlers (LGWs). An automatic algorithm is developed to identify burst mode waveform data with LGW signals and analyze the wave polarization information for these LGW signals. The spatial distribution of the LGW occurrence and the probabilities of different propagation types demonstrate that most LGWs can be observed in the low *L*-shell region (L < 3), where the dominant propagation type is oblique outward. Parallel propagation dominates in the high *L*-shell region, but the LGW occurrence is very small. Additionally, a small group of oblique but inwardly propagating LGWs are observed at low altitudes ($<0.2R_E$). A ray tracing simulation is performed not only to confirm predominant oblique and outward wave vectors in the vast region of the plasmasphere but also to verify the existence of these inward propagating LGW signals at low altitudes near the topside ionosphere.

Plain Language Summary A fraction of broadband electromagnetic emissions produced by lightning strikes in the Earth's atmosphere can propagate through the ionosphere into the magnetosphere as lightning-generated whistlers (LGWs). The LGW plays an important role in the electron scattering of the radiation belts, the efficiency of which highly depends on their wave normal angles and thus the propagation modes of the LGWs. In this study, we develop an algorithm to identify the burst mode waveform data from Van Allen Probes' observations that capture the LGW signals. Using these identified waveforms, we statistically study the wave normal distribution for LGWs in the inner magnetosphere. The results indicate that most LGWs are observed in the low altitude region ($<2R_E$, R_E is the Earth's radius) with an oblique, radially outward wave normal. In the high altitude region ($<3R_E$), parallel wave normals dominate, and in the very low altitude region ($<0.2R_E$), the oblique inward wave normal exists. A ray tracing simulation is performed to confirm the dominant oblique wave normal of LGWs and the existence of inward wave normals caused by the great plasma density gradient in the very low altitude region. The results lead to our systematic understanding of LGWs and advance the predictive capability of radiation belts.

1. Introduction

Lightning strikes in the Earth's atmosphere can produce broadband electromagnetic emissions, which are mostly confined in the waveguide between the Earth and the ionosphere, within a horizontal distance of up to \sim 1,000 km from the corresponding lightning sources (Fiser et al., 2010). Part of this lightning-associated radiation can leak through the ionosphere within a narrow transmission cone near the vertical direction (Santolík et al., 2009) and propagate into the inner magnetosphere as lightning-generated whistler (LGW) waves (Carpenter, 1968; Clilverd et al., 2008; Helliwell, 1965, 1969; Inan & Bell, 1977; Storey, 1953; Tao et al., 2010). LGW waves are coherent emissions with a frequency range from \sim 100 Hz to >30 kHz (Marshall et al., 2021), and most LGW waves are confined inside the plasmasphere (Bortnik et al., 2003a; Oike et al., 2014). LGW waves are suggested to make a significant contribution to the electron scattering in the inner radiation belt and slot region (the region separating the inner and outer radiation belts) (Abel & Thorne, 1998; Gemelos et al., 2009; Green et al., 2020; Inan et al., 2007; Peter & Inan, 2005; Rodger et al., 2003).

Recent studies compare observations from the World Wide Lightning Location Network (WWLLN) on the ground to the in-situ spacecraft' observations either at the topside ionosphere (DEMETER satellite) or near the equatorial magnetosphere (Van Allen Probes), and reveal a significant correlation between lightning activity and magnetospheric whistler waves. Němec et al. (2010) found good agreement between the lightning activity recorded on the ground and the electric field fluctuations above 2 kHz observed by the DEMETER satellite. The

© 2024. American Geophysical Union. All Rights Reserved.

XIA ET AL. 1 of 12

LGW wave intensity is stronger at the nightside than the dayside (because of much weaker collisional damping at the nightside) and is larger in summer (due to higher occurrences of lightning strokes). A conjugate observation (Zheng et al., 2016) reveals that approximately 40% of the whistlers observed by Van Allen Probes are one-to-one coincident with source lightning strikes observed by WWLLN within 2,000 km of the Van Allen Probes footprint. Recently, Ripoll et al. (2020) compared the distribution of the LGW distribution observed from Van Allen Probes in longitude, L-shell and magnetic local time (MLT) with the distribution of lightning power density calculated from WWLLN and found a great agreement for the region of L > 2.

From the observations of the DEMETER satellite, Colman and Starks (2013) found that LGW magnetic power maximizes between $L \sim 1.5$ and $L \sim 2.2$ with a plateau at $L \sim 2$, and decays below $L \sim 1.5$. Using this wave model as the source at the DEMETER altitude, Starks et al. (2020) traced the wave propagation and wave power variation to obtain a model of LGW wave intensity inside the magnetosphere. Compared with the existing empirical LGW intensity (from CRRES mission (Meredith et al., 2007) and from AKEBONO (Agapitov et al., 2014)), the modeled LGW wave intensity shows an inconsistent L-shell profile and is lower in magnitude (Figure 18 of Starks et al. (2020)). As Starks et al. (2020) argued, previous empirical LGW wave models in space may be overestimated by a factor of ~ 2 to 10, especially in the large L-shell region (L = 2 - 4), due to the difficulty in distinguishing them from plasmaspheric hiss with adjacent or overlapping frequency range. Green et al. (2020) used the waveform observations of Van Allen Probes to extract LGW signals and statistically studied the distribution of LGW wave power in the inner magnetosphere. Their results indicate that the LGW amplitude is strong at L < 3 and that the occurrence is higher at the nightside than at the dayside. Recently, Ripoll, Farges, Malaspina, Cunningham, Lay, et al. (2021) reported observations from both ground (by WWLLN) and space (by Van Allen Probes) during lightning superbolts and found several properties of superbolts that are different from usual lightning flashes: a more symmetric first ground-wave peak, larger peak electric current, weaker decay of electromagnetic power density in space with distance, and more confined wave power in the very low frequency

LGW waves can propagate in ducted or nonducted modes (Carpenter, 1968; Clilverd et al., 2008; Helliwell, 1969; Inan & Bell, 1977). The ducted mode, through which the waves propagate along the background magnetic field line, requires the existence of fine-scale gradients of the plasma density (Streltsov, 2021a, 2021b, 2022; Streltsov et al., 2006). In such a mode of propagation, LGW-induced pitch angle scattering of electrons may be more effective since the wave normal angles remain small. In theory, the ducted mode is more favorable for whistler waves below $f_{ce}/2$ (Liu et al., 2021; Smith, 1961; Smith et al., 1960), where f_{ce} is the electron gyrofrequency, and thus, the comparison between the wave frequency and $f_{ce}/2$ is often used as the indirect indication for the ducted mode. The nonducted mode takes place in a smoothly varying medium. The wave normal angle analysis of the LGW in Green et al. (2020) indicates that there exists a mixture of ducted and nonducted LGWs at L < 2 and below $0.25 f_{LHR}$ over 2 < L < 4, and the nonducted mode becomes dominant over the range f_{LHR} to $0.1 f_{CC}$ over 2 < L < 4. Recently, Ripoll, Farges, Malaspina, Cunningham, Hospodarsky, et al. (2021) used survey-mode spectral data of Van Allen Probes to perform a statistical study of the wave normal angle distribution in the region L < 3. They found that the distribution of predominantly electrostatic waves peaked at a large wave normal angle, while the distribution of electromagnetic waves with a large magnetic component and small electric component peaked at a small wave normal angle. The seasonal and continental dependences of the wave normal angle were found to be very weak.

In previous studies about the LGWs from the Van Allen Probes observation, the identification of LGW signals was mainly based on the filter of the signal-to-noise ratio (SNR) of either the survey spectra data (Ripoll, Farges, Malaspina, Cunningham, Hospodarsky, et al., 2021) or burst mode waveform data (Green et al., 2020), which may include many non-LGW noises. Additionally, the LGW data in these studies are confined to a limited L-shell range (L < 3 in Ripoll, Farges, Malaspina, Cunningham, Hospodarsky, et al. (2021) and L < 4 in Green et al. (2020)). In this study, we develop a new identification algorithm based on the frequency dispersion of the LGW signals and select the EMFISIS burst mode waveform data of Van Allen Probes with LGW signals. Consequently selected LGW data are not confined to a limited L-shell region. Using these identified LGW signals, we perform a detailed analysis of the wave normal angle distribution of the LGWs in the inner magnetosphere and its association with various modes of wave propagation (such as ducted and nonducted modes). Finally, a ray tracing simulation is used to understand the propagation characteristics. In this paper, we focus on wave normal direction characteristics instead of the direction of Poynting vectors and

XIA ET AL. 2 of 12

we use propagation direction in general to denote wave normal direction unless it is explicitly mentioned otherwise.

2. Spacecraft and Instruments

The Van Allen Probes mission (Mauk et al., 2013) consists of twin satellites with identical instruments with nearly similar near-equatorial and highly elliptical orbits with a perigee of approximately $1.1R_E$ and an apogee of approximately $5.8~R_E$. They were launched in August 2012 and decommissioned in October 2019, with an operating duration of approximately 7 years. The Waveform Receiver (WFR) of the Electric and Magnetic Field Instrument Suite and Integrated Science (EMFISIS) (Kletzing et al., 2013), consisting of six identical waveform receivers with flat (to within 1 dB) response from 10 Hz to 12 kHz, provides 6-s duration of continuous burst-mode waveform measurements of six electromagnetic components. The receivers are followed by a bandpass filter (10 Hz-12 kHz) and a 16-bit A/D converter is used to digitize each signal at a sampling rate of 35 kHz. The waveform data can be transferred from the satellite's coordinates ("uvw" coordinates) into the Geocentric Solar Ecliptic (GSE) coordinates. Combining with the background magnetic field and satellite's location measurements in the GSE coordinates, we can obtain the wave propagation and polarization information in the field-aligned coordinates (FAC).

3. Identification and Polarization Analysis of the Lightning-Generated Whistler

An algorithm is developed to identify time intervals of the Van Allen Probes EMFISIS WFR burst mode waveform data with LGW signals, and is explained by the following steps. First, for a set of 6-s magnetic field waveform data (e.g., the waveform observed by Van Allen Probes B on 12 October 2017, shown by Figure 1), fast Fourier transformation (FFT) is performed to obtain the wave total magnetic power spectral density (Figure 1a), and the corresponding signal-to-noise ratio (SNR) (Figure 1b) is calculated using the mean value of a moving time window of ~ 0.09 s as the background noise power. Then, the SNR spectra are converted into binary spectra (with a value of 1 representing SNR ≥ 10 and 0 otherwise). For these binary-value dynamic spectra, the frequency dispersion effects of LGW signals (i.e., higher frequency signals are observed earlier than lower frequency signals) are removed so that the LGW signals can be converted to vertical stripes. The method of removing frequency dispersion is also known as the dechirping algorithm in Zheng et al. (2016); Jacobson et al. (2011). An example of resultant vertical binary-value spectra (PSD^*) is shown in Figure 1c. Using PSD^* , we summed over the frequency and found local peaks. If a peak value (representing the number of frequency bins) exceeds a threshold value, then this local peak is identified as an LGW signal (Figure 1d). The red dashed line in Figure 1d is the threshold value to determine an LGW element in this event, and the identified LGW elements are labeled by the white dashed lines in Figure 1c. One can see that strong LGW elements are effectively identified.

Using the algorithm above, we have identified waveforms with at least one LGW signal as our database for this study. From all 7 years of 2,903,610 waveforms data of both Van Allen Probes A and B, 105,383 waveforms with LGW signals are automatically identified. After manual inspection, only 284 waveforms were found to be falsely identified, and 105,099 waveforms with clear LGW signals were correctly identified, with a very high correct identification rate of 99.73%. These identified burst-mode waveform data were then used to extract propagation and polarization features of LGW waves, using the singular value decomposition (SVD) method (Santolík et al., 2003). For the example waveform shown in Figure 1, panels 1e-1h show the polar angle (θ_h) and the azimuthal angle (ϕ_k) of the wave vector **k** and the polar angle (θ_P) and the azimuthal angle (ϕ_P) of the Poynting vector **P**, respectively. The signals with magnetic field wave power spectral density less than $10^{-8} nT^2/Hz$, ellipticity less than 0.7, or planarity less than 0.7 are filtered out in Figure 1e-1h. The polar angles and azimuthal angles are defined in the field-aligned coordinates (FAC), in which the z-axis is along the direction of the background magnetic field, the y-axis is along the direction of the cross product of the z-axis and the radial direction (from the Earth's center to the satellite), and the x-axis is the cross product of the y-axis and z-axis. The waveform analysis shows a series of LGW signals with clear frequency dispersion. This 6-s waveform reveals a series of pulses with oblique wave normal angle (130° $< \theta_k < 170^\circ$) and inward pointing wave vector $(\phi_k \sim \pm 180^\circ)$. The characteristics of inward wave vectors will be further discussed in the following sections. The Poynting vector shows that the LGW propagates southward nearly along the background field line (Figure 1g) and inward (Figure 1h). A similar analysis to this example case was performed for all waveform data from Van Allen Probes with identified LGW signals, and we conducted a statistical study on the LGW propagation characteristics in the inner magnetosphere.

XIA ET AL. 3 of 12

21699402, 2024, 4, Downloaded from https://agupubs.onlinelibrary.wiley.com/doi/10.1029/2023IA03333 by British Antarctic Survey, Wiley Online Library on [29.09/2025]. See the Terms and Conditions (https://onlinelibrary.wiley.com/etms-and-conditions) on Wiley Online Library for rules of use; OA articless

are governed by the applicable Creativ

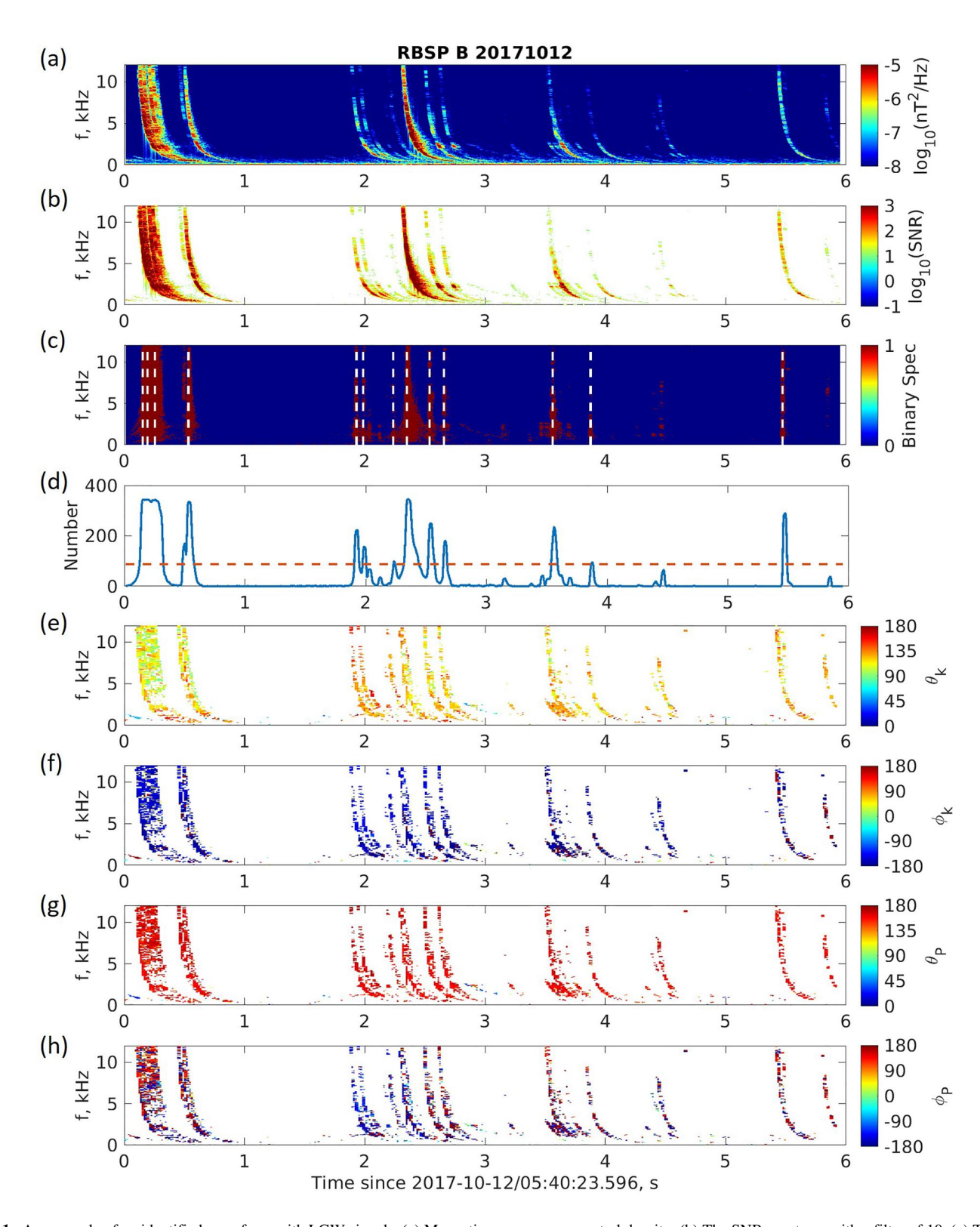


Figure 1. An example of an identified waveform with LGW signals. (a) Magnetic wave power spectral density. (b) The SNR spectrum with a filter of 10. (c) The best transformed binary spectrum and (d) the sum over frequency versus time of the transformed binary spectrum. (e) Polar angle, and (f) azimuthal angle of the wave normal vector. (g) Polar angle and (h) azimuthal angle of the Poynting vector.

XIA ET AL. 4 of 12

21699402, 2024, 4, Downloaded from https://agupubs.onlinelibrary.wiley.com/doi/10.1029/2023JA032333 by British Antarctic Survey, Wiley Online Library on [29/09/2025]. See the Terms and Conditions

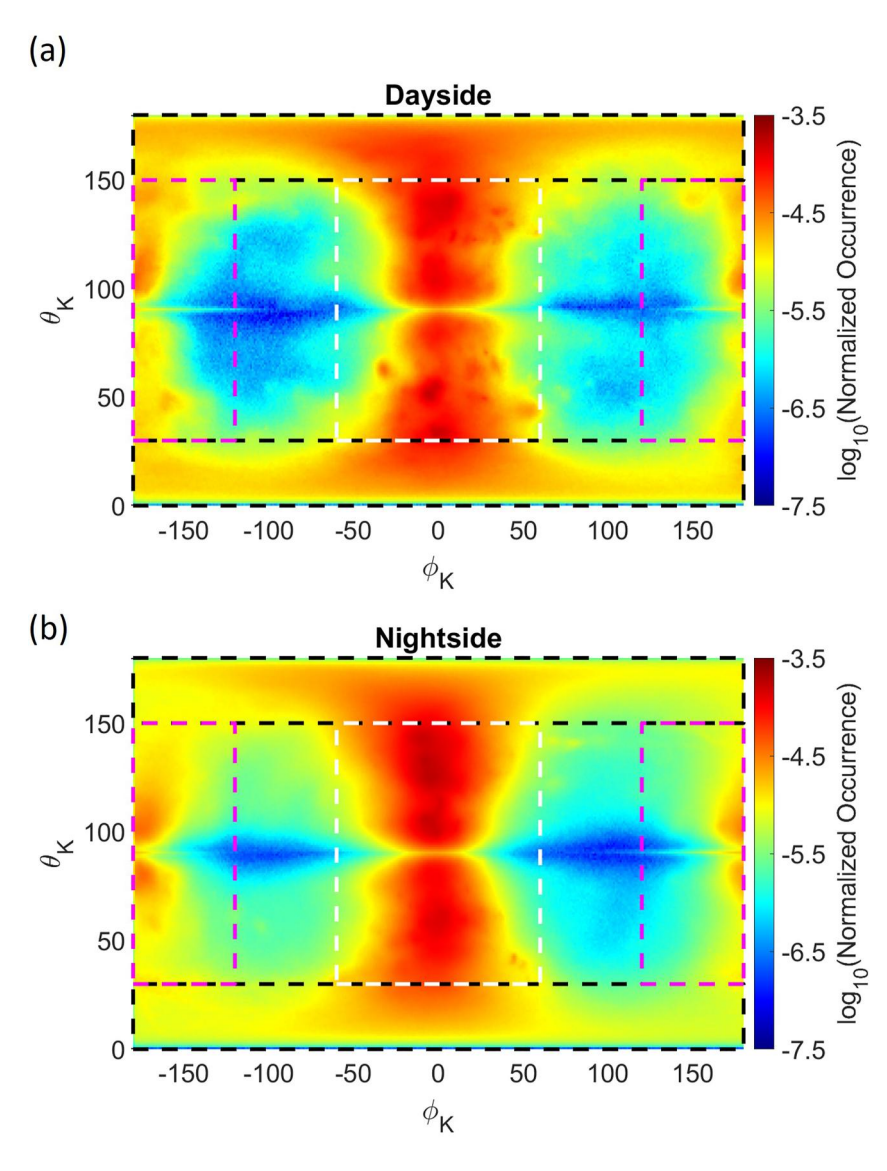


Figure 2. The distribution of the normalized occurrence of data points for different polar angles and azimuthal angles of the wave vector for the (a) dayside (6–18 MLT) and (b) nightside (18–24 and 0–6 MLT). The black, white and magenta dashed boxes label the quasi-parallel, obliquely outward and obliquely inward propagation data points, respectively.

4. Statistical Results of the LGW Distribution and Propagation

Using the 105,099 identified 6-s waveforms with LGW signals from ~7 years of observation of Van Allen Probes, we performed propagation analysis and then derived the spatial distribution of the LGW propagation features in the inner magnetosphere. A total of 2,752 waveforms (2.62%) were ignored due to the lack of other supportive data, such as the background magnetic field and coordinate transformation information. To examine the statistical characteristics of θ_k and ϕ_k of the LGW signals, we plotted the distribution of the normalized occurrence of the data points for LGW signals over the frequency range between 2 and 10 kHz over θ_k and ϕ_k for the dayside (Figure 2a) and the nightside (Figure 2b), respectively. The data points of LGW signals were selected by applying the same filters as Figures 1e–1h to the waveform spectra. It should be noted that ϕ_k loses its meaning for nearly parallel ($\theta_k = 0^\circ$) and antiparallel ($\theta_k = 180^\circ$) wave vectors. We find that most LGW signals are confined near the meridian plane with a preferred direction of radially outward ($\phi_k \sim 0^\circ$). The θ_k is widely distributed from near parallel ($\sim 10^\circ$ and $\sim 170^\circ$) to almost perpendicular ($\sim 90^\circ$), with peak occurrences at $\sim 40^\circ$ –80° and $\sim 100^\circ$ –150°. In addition to the dominant occurrences of radially outward propagation ($\phi_k \sim 0^\circ$), there is also a considerable number of occurrences with oblique radially inward propagation ($\phi_k \sim 1180^\circ$). The outward propagation

XIA ET AL. 5 of 12

direction is expected in the nonducted propagation of whistler mode waves in the magnetosphere due to the Earth's magnetic field, which tends to refract the wavenumber vectors away from the Earth. A similar angular distribution with dominant outward propagation was reported for chorus waves in the magnetosphere (Hartley et al., 2019), which can be explained by the same propagation effect. The existence of the inward propagation mode is rather unexpected, and we will perform a detailed analysis of the origin of these waves in the next section.

From the θ_k and ϕ_k distribution shown in Figure 2, we can divide the wave propagation into three main sub_regions: (a) quasi-parallel propagation ($\theta_k < 30^\circ$ or $\theta_k > 150^\circ$, labeled by the black dashed boxes in Figure 2); (b) obliquely outward propagation ($30^{\circ} < \theta_k < 150^{\circ}$ and $|\phi_t| < 60^{\circ}$, labeled by the white dashed boxes in Figure 2); and (c) obliquely inward propagation (30° $< \theta_k < 150^\circ$ and $|\phi_k| > 120^\circ$, labeled by the magenta dashed boxes in Figure 2). Using these analyzed waveforms, we can check the spatial distribution of different propagation modes. We first check the distribution of the occurrence rate of observed LGW signals. The occurrence rate is obtained as the number of filtered LGW spectral data points normalized by the total number of spectral data points for all the burst mode waveform measurements $(n_{wf} \times n_t \times n_f)$ where n_{wf} is the number of 6-s waveform measurements (shown in the Supporting Information), $n_r = 406$ and $n_f = 511$ are, respectively, the numbers of the time bins and frequency bins of a 6-s spectrum due to a single waveform). The equatorial and meridional distributions of this LGW occurrence rate are shown in Figures 3a and 3b, respectively. The radial component in the equatorial distribution (Figure 3a) is the L-shell, while in the meridional distribution (Figure 3b), the radial component is the geocentric distance. The results indicate that most LGWs are observed in the region of L < 3, and that more LGWs can be observed at the nightside than at the dayside, as expected due to less electron collisional damping through the nightside D-region ionosphere (e.g., Tao et al., 2010). The dependence of the occurrence rate on the latitude is not very significant. Few LGW signals can be observed at L > 5. For the filtered LGW data points in each spatial bin, the proportions of the data points for each of the three propagation modes, outward, inward and parallel propagation, are calculated to approximate the probabilities of corresponding propagation modes as a function of location. Figures 3c-3h show the equatorial and meridional distributions of the probabilities for outward propagation (3c, 3d), inward propagation (3e, 3f), and parallel propagation (3g, 3h) signals. The results show that at a large L-shell (>~4), most LGWs propagate nearly parallel to the background magnetic field. The lower obliqueness may be due to the following two factors: (a) the plasmapause can be a very structured boundary layer with many density crests and troughs to guide the LGWs; (b) most observed LGW signals in this region are those guided from near-ground sources without experiencing magnetospheric reflection in the inner magnetosphere. In contrast, at L < 3, most LGWs propagate obliquely, especially near the equator. Most of the oblique propagation corresponds to outward wave normal vector direction, while inward propagation (with inward wave normal direction) only becomes significant in the low altitude ($<0.2R_F$) region, with slightly more preference at the dayside than nightside. This day-night asymmetry of inward propagation may be caused by the larger scale height of the plasma density profiles in the ionosphere at the dayside than the nightside, and the resulting broader regions of large density gradient at low altitudes are favorable for the inward propagation of the whistler wave. We will look into the mechanism of inward and outward propagation modes in the next section.

Here we examine the wave normal angle distribution at different frequencies. Figure 4a shows the occurrence rate of different wave normal angles θ_k (y-axis) within different frequency bins (x-axis), which is calculated by the data point number of a θ_t -frequency bin dividing the total data point number of the corresponding frequency bin. Similar to the result in Figure 2, the values of wave normal angles exhibit a wide spread from nearly parallel to very oblique with the occurrence peaks near 30° and 150° for all the frequency bands. The occurrence gap near 90° becomes wider as frequency increases, due to wider resonance cone at higher wave frequency. In the low frequency bands (~2-6 kHz), there exists a secondary peak in occurrences close to 90°. The frequency-dependent wave normal angle distributions may reflect different types of LGW signals over different frequency ranges. In these observed LGW cases, there are three main types of LGW signals: (a) the original LGW signals before any reflection (Figure 1), which are usually observed in low L-shell region $(L < \sim 3)$ with a wide range of wave normal angles over the entire frequency band; (b) the nose whistlers (Helliwell, 1965), which are observed at high L-shell region $(L > \sim 3)$ with near parallel wave normal angles in low frequency range (with a frequency upper bound near the nose frequency); (c) the magnetospheric reflected (MR) whistlers (Bortnik et al., 2003b; Edgar, 1976), which are the manifestation of original LGWs after multiple magnetospheric reflections and are usually observed in the low L-shell region with very oblique wave normal angles in low frequency range. The secondary peak near 90° in Figure 4a should be mainly contributed by the MR whistlers.

XIA ET AL. 6 of 12

21699402, 2024. 4, Downoaded from https://agupubs.onlinelibrary.wiley.com/doi/10.1029/20214032353 bg fritish Antarctic Survey, Wiley Online Library on [2909/2025]. See the Terms and Conditions (https://onlinelibrary.wiley.com/rems-and-conditions) on Wiley Online Library for rules of use; OA articles are governed by the applicable Creative

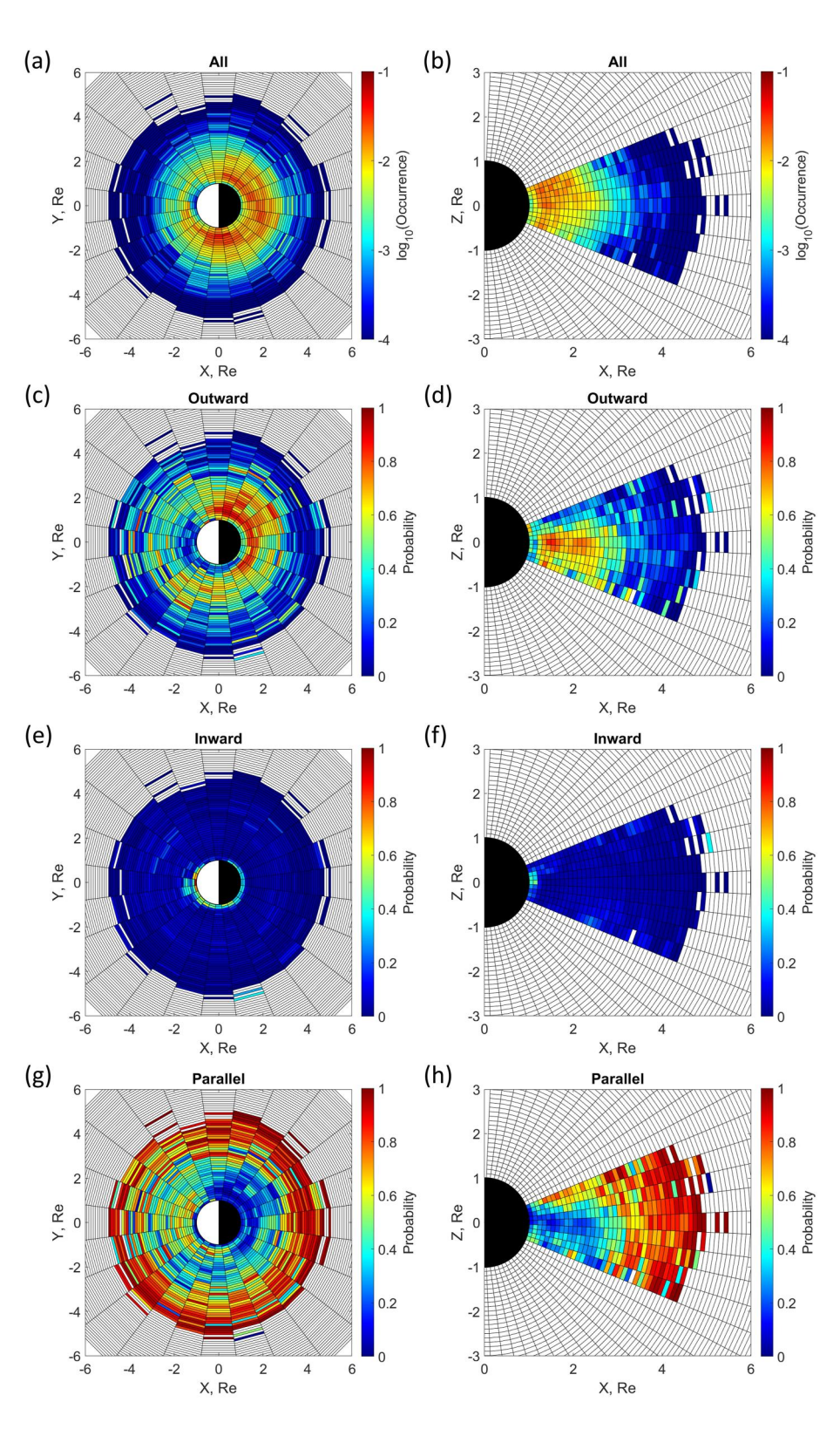


Figure 3. (a) and (b) are the distributions of the LGW occurrence in the equatorial and meridional planes, respectively. (c) and (d) are the distributions of the probability of the oblique outward propagating LGW signal in the equator and meridional planes, respectively. (e) and (f) are the distributions of oblique inward propagation. (g) and (h) are the distributions of parallel propagation. The radial component in the equatorial plane is the L-shell, while in the meridional plane is the geocentric distance.

XIA ET AL. 7 of 12

21699402, 2024, 4, Downl

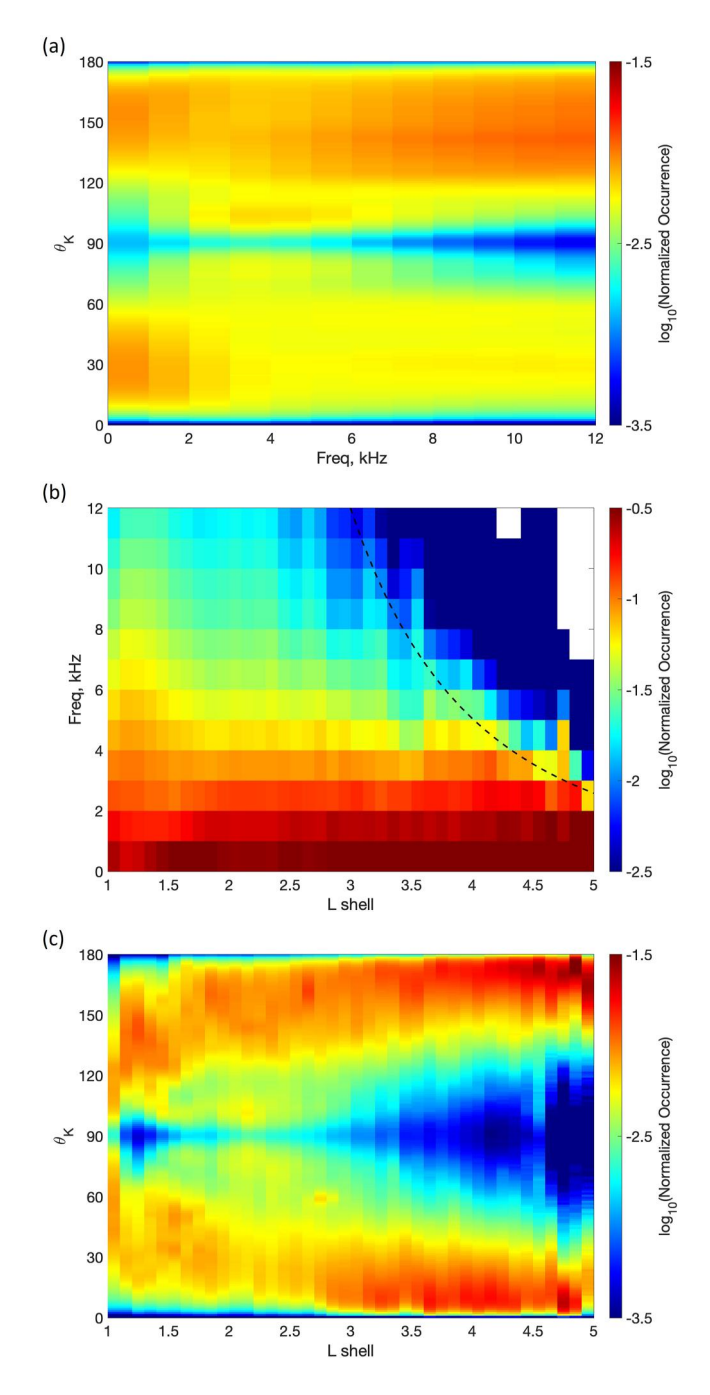


Figure 4. (a) The occurrence rate of LGW signals with different wave normal angle θ_k (y-axis) in different frequency bins (x-axis). (b) The occurrence rate of LGW signals with different wave frequencies (y-axis) in different L-shell bins (x-axis). (c) The occurrence rate of LGW signals with different wave normal angles θ_k (y-axis) in different L-shell bins (x-axis).

To further check the distribution of the three main types of LGW signals, we make another two plots. The first one is the occurrence rate of different frequencies (y-axis) within different L-shell bins (x-axis), which is calculated by the data point number of a frequency-L bin dividing the total data point number of the corresponding L-shell bin. A clear frequency upper bound can be found in the large L-shell region and the frequency bound decreases as the L value increases. We overplot the estimation of the nose frequency $(0.37f_{co})$ (Angerami & Carpenter, 1966; Ho & Bernard, 1973) as the black dashed line, and the variation of the nose frequency matches the frequency upper bound well. This suggests that the main LGW signals in the large L-shell region are nose whistlers. In the low L-shell region, there is a mixture of original LGWs and MR whistlers. The occurrence rates of the higher frequency bands (>6 kHz) are lower than the lower frequency bands (<6 kHz), likely due to the two following reasons: (a) the intensity of the higher frequency band is weaker; (b) the MR whistlers have an upper frequency bound. Figure 4c shows the occurrence rates of different wave normal angles θ_k (y-axis) within different L-shell bins (x-axis), which is calculated by the data point number of a θ_k -L bin dividing the total data point number of the corresponding L-shell bin. The wave normal angle distribution spreads widely when L-shell is small (L < 3) and tends to be more parallel as the L-shell increases. Also, a considerable population of MR whistlers with very oblique wave normal angles can be found in the low L-shell region.

5. Inward and Outward Propagation Modes of LGWs

To understand the inward and outward propagation modes of LGWs, we conducted a ray tracing simulation. We used the HOTRAY ray tracing code (Horne, 1989) with a dipole magnetic field and a diffusive equilibrium plasma density model with the parameters for the dayside as described in Bortnik et al. (2011). Ray tracing in such a medium simulates propagation characteristics of the nonducted propagation mode. The rays are launched at an altitude of 500 km, with a typical LGW frequency of 5 kHz and the initial wave normal being radially outward (since the transmission cone is very close to the vertical direction (Bortnik et al., 2006; Helliwell, 1965)) at different magnetic latitudes in the Northern Hemisphere. The L-shell of the plasmasphere is set to be an artificially high value of 10 so that we can compare the propagation paths over a large range of L within the plasmasphere. The results of the ray tracing simulation are shown in Figure 5. Figure 5a shows the distribution of the plasma density on the meridional plane. One important feature is the presence of a strong vertically downward gradient of plasma density in the low altitude region associated with the ionospheric density peak. Figure 5b shows the ray paths launched from different latitudes (denoted by colors) on the meridional plane, with the portion of inward (outward) wave vector direction represented by thick (thin) line segments. The short black lines with circles label the direction of the wave vector at different points (the circles) along the ray paths. Figure 5c, zoom-in of Figure 5b and provides a clearer view of the obliquely inward propagation in the low altitude regions labeled by the navy thick line segments. The varia-

tions in the radius, L-shell and wave normal angles θ_k of the ray paths are shown in Figures 5d-5f, respectively. Similar to Figure 5b, the thin (thick) line segments in Figures 5d and 5e denote the outward (inward) wave normal direction. The rays can propagate upward from the ionosphere into the inner magnetosphere. Rays launched within 10° of the equator can only propagate up to a limited altitude (corresponding to $L \sim 1.5$) and then refract downward to the Earth, while rays launched at higher latitudes can propagate beyond $L \sim 1.5$ and continue to propagate outward after magnetospheric reflection in the Southern Hemisphere when the wave frequency falls just below the local lower hybrid resonant frequency f_{LHR} . For the rays initialed from higher latitudes, the wave

XIA ET AL. 8 of 12



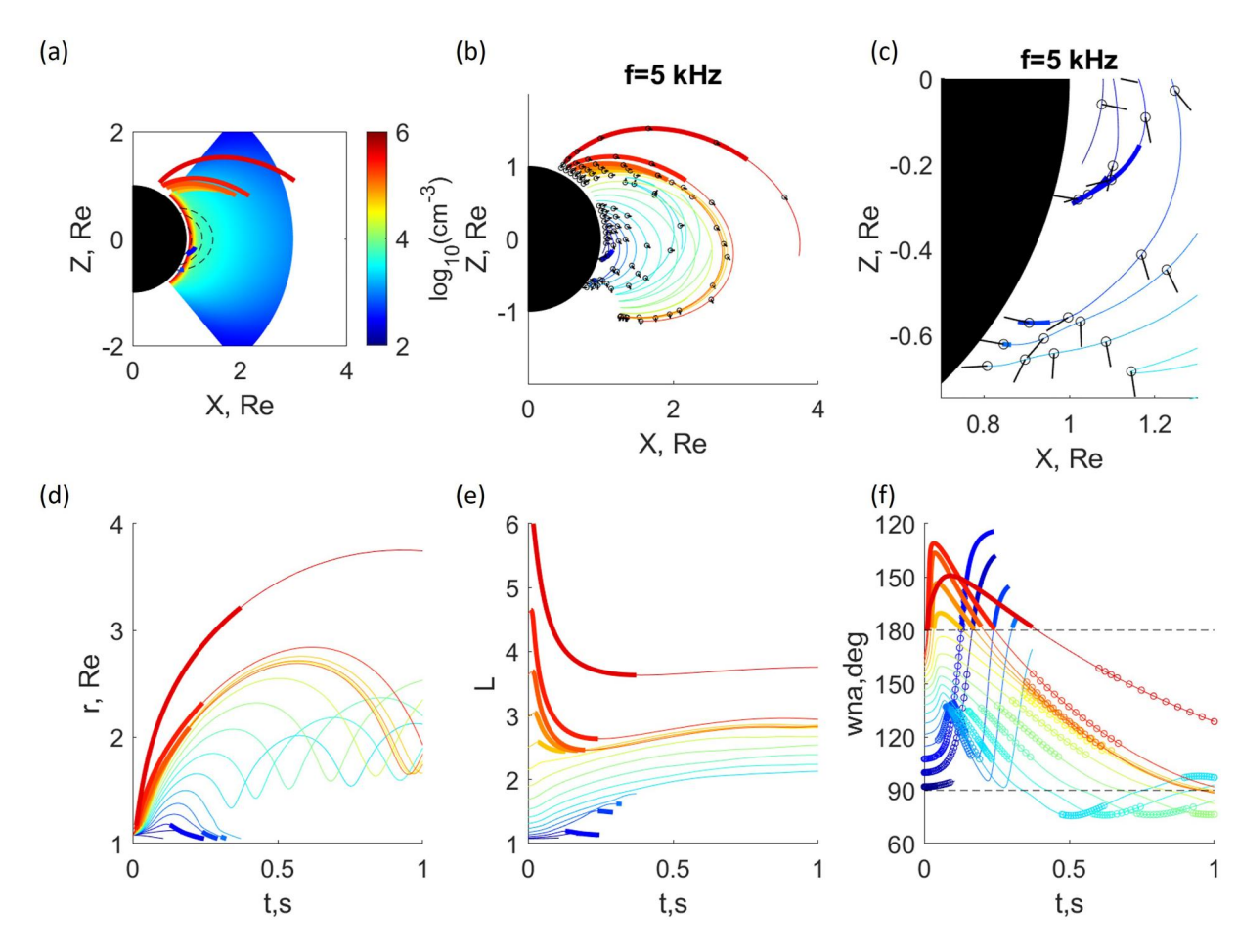


Figure 5. (a) The meridional distribution of electron density used for the ray tracing model. (b) The paths of the rays starting from different initial latitudes (denoted by colors). (c) Is the zoomed-in view of (b). (d) to (f) are the variations of radial distance (d), L-shell (e), and wave normal angle (f), versus propagation time in seconds, respectively. The two horizontal dashed lines in (f) denote the wave normal angles of 90° and 180°, respectively. The dashed black lines in (a) represent dipole field lines at L = 1.1, 1.3 and 1.5, respectively. The thin (thick) lines in (b) to (f) denote the outward (inward) propagation direction. The black short lines with circles in (b) and (c) label the directions of the wave normal vectors. The colored hollow circles in (f) label the region with altitude <10°.

normals initially point inward at the high latitude region. This simulated inward propagation can not be verified by the observation of Van Allen Probes due to the limited inclination of their orbits. As the rays propagate to the low latitude region, their wave normals become progressively oblique outward near 90°. These rays occupy most of the equatorial plasmaspheric region with outward wave normals and oblique wave normal polar angles, which is consistent with the observation of dominant occurrences of oblique and outward k vectors. In contrast, for the rays starting within $\sim 10^{\circ}$ near the equator, the wave normals initially are directed outward and then turn inward, leading to the confinement of the inward wave normals within $<20^{\circ}$ of the equatorial region below $1.2R_{E}$. The spatial region of these inward k vectors from the ray tracing simulation coincides with that of the inward propagating LGW signals observed by Van Allen Probes (Figure 3). This unexpected inward propagation mode is a consequence of inward refraction by a strong downward density gradient in the topside ionosphere, which is similar to the ducting effect of the strong inward density gradient at the plasmapause. To demonstrate this, we overplot the portion of inward propagating rays (thick lines in Figure 5b) onto Figure 5a. One can observe that the region of inward propagation coincides with the topside ionosphere with a strong density gradient (plasma density varying from $\sim 10^6$ to $\sim 10^4$ cm⁻³ from 300 km to 1,300 km in altitude). Therefore, both the inward and outward oblique propagations are mostly a result of the nonducted propagation mode. A special case is that some LGWs with very oblique wave normal angles near the Gendrin angle can also be ducted by the plasma troughs (Helliwell, 1965).

Besides verifying the occurrence of the inward propagation of the LGW signals in the very low altitude region, we also compare the wave normal angles in the equatorial plasmasphere region between the ray tracing simulation

XIA ET AL. 9 of 12

and our observation results. We label the wave normal angles in the region with latitude $<10^{\circ}$ as the hollow circles in Figure 5f. The values of the wave normal angles range from nearly parallel to very oblique in the low L-shell region (L < 3) and become more parallel in the high L-shell region (the red lines), which are consistent with the statistical results from the observations. Moreover, the MR whistlers are also reproduced by the ray tracing simulation. The rays with cyan and green colors propagate from the North Hemisphere to the South Hemisphere and then reflect back to the North Hemisphere in the low L-shell region. The waver normal angles after the reflection become very oblique, which coincides with the population of the observed very oblique wave normal angles associated with the MR whistlers. Moreover, we also checked the ray tracing results of waves with lower and higher frequencies (2 and 8 kHz). For different frequencies, the ray tracing results do not show much difference. Thus, we include the ray tracing results of 2 and 8 kHz waves in the supporting information as Figures S2 and S3 in Supporting Information S1.

6. Conclusions and Discussion

In this study, we use approximately 7 years of observations from Van Allen Probes to statistically analyze the propagation features of lightning-generated whistlers (LGWs) in the inner magnetosphere. We develop an automatic method to identify the 6-s Van Allen Probes EMFISIS WFR waveform data that contain the LGW signals and apply the singular value decomposition (SVD) methods to obtain the polarization and propagation information of the LGW waves. Wave normal direction observations are compared directly against ray tracing simulations. The main conclusions are summarized as follows.

- 1. Most LGW signals are more likely to be observed at the nightside within the region of L < 3.
- 2. At large $L(L \sim 4)$, the dominant propagation type is parallel propagation (ducted propagation mode), while in the lower L-shell region, most of the propagation becomes oblique (nonducted propagation mode), with dominant azimuthal direction being outward.
- 3. An unexpected population of obliquely inward propagating LGW signals is observed. The inward propagating LGW waves are confined at very low altitudes ($<0.2R_E$) near the equator.
- 4. Our ray tracing simulation not only accounts for the dominant outward signals in the plasmasphere, but also confirms the existence of inward propagating signals confined at region with altitude $<0.2R_E$. The inward signals are attributed to the refraction associated with a downward density gradient in the topside ionosphere.

Due to the constraint of Van Allen Probes' low inclination orbits, only the LGW waves within 20° of the equator are available in this work. Within this limited latitude range, the statistical result still shows some latitudinal variation of the wave normal angle distribution. As shown in Figures 3d and 3h, we can see that in the North Hemisphere, the wave normal direction is more parallel compared to the South Hemisphere. The reason for this latitudinal variation might be more lightning activities in the North Hemisphere (Němec et al., 2010). The wave normal angle increases during the propagation and becomes very oblique after crossing the equator. The ARASE (also known as Exploration of energization and Radiation in Geospace) satellite (Miyoshi et al., 2018), which orbits at a higher inclination and covers magnetic latitudes up to $\sim 40^{\circ}$, will greatly supplement the current study to examine the LGW wave propagation characteristics of LGWs over regions of relatively large latitude. This will be left as a follow-up study of this paper.

The results in this study are also relevant to the question of whether the LGW propagates in ducted or non-ducted modes in the inner magnetosphere. The dominant occurrence of LGW waves with radially outward propagation is a signature of nonducted propagation. Even a secondary group of inward propagations at low altitudes can be explained by nonducted propagation mode. Understanding the distribution of the LGW's wave normal direction can help improve the evaluation of the electron loss in the inner magnetosphere, which will expand our knowledge about the link between near-ground atmospheric activity and the radiation environment in space.

Data Availability Statement

The data of Van Allen Probes used in this paper were provided by the Space Physics Data Facility (SPDF) https://spdf.gsfc.nasa.gov/pub/data/rbsp/.

XIA ET AL. 10 of 12

Acknowledgments

We acknowledge the support of NASA grants 80NSSC22K1637, 80NSSC29K324, 80NSSC19K0282 and 80NSSC21K0728. RBH was supported by NERC Highlight Topic Grant NE/P01738X/1 (Rad-Sat) and NERC grant NE/V00249X/1 (Sat-Risk).

References

- Abel, B., & Thorne, R. M. (1998). Electron scattering loss in earth's inner magnetosphere: 1. Dominant physical processes. *Journal of Geophysical Research*, 103(A2), 2385–2396. https://doi.org/10.1029/97JA02919
- Agapitov, O. V., Artemyev, A. V., Mourenas, D., Kasahara, Y., & Krasnoselskikh, V. (2014). Inner belt and slot region electron lifetimes and energization rates based on akebono statistics of whistler waves. *Journal of Geophysical Research: Space Physics*, 119(4), 2876–2893. https://doi.org/10.1002/2014JA019886
- Angerami, J. J., & Carpenter, D. L. (1966). Whistler studies of the plasmapause in the magnetosphere: 2. Electron density and total tube electron content near the knee in magnetospheric ionization. *Journal of Geophysical Research* (1896-1977), 71(3), 711–725. https://doi.org/10.1029/JZ071i003p00711
- Bortnik, J., Chen, L., Li, W., Thorne, R. M., & Horne, R. B. (2011). Modeling the evolution of chorus waves into plasmaspheric hiss. *Journal of Geophysical Research*, 116(A8), A08221. https://doi.org/10.1029/2011JA016499
- Bortnik, J., Inan, U. S., & Bell, T. F. (2003a). Energy distribution and lifetime of magnetospherically reflecting whistlers in the plasmasphere. Journal of Geophysical Research, 108(A5), 1199. https://doi.org/10.1029/2002JA009316
- Bortnik, J., Inan, U. S., & Bell, T. F. (2003b). Frequency-time spectra of magnetospherically reflecting whistlers in the plasmasphere. *Journal of Geophysical Research*, 108(A1), 1030. https://doi.org/10.1029/2002JA009387
- Bortnik, J., Inan, U. S., & Bell, T. F. (2006). Temporal signatures of radiation belt electron precipitation induced by lightning-generated mr whistler waves: 1. Methodology. *Journal of Geophysical Research*, 111(A2), A02204. https://doi.org/10.1029/2005JA011182
- Carpenter, D. L. (1968). Ducted whistler-mode propagation in the magnetosphere; a half-gyrofrequency upper intensity cutoff and some associated wave growth phenomena. *Journal of Geophysical Research* (1896-1977), 73(9), 2919–2928. https://doi.org/10.1029/JA073i009p02919
- Clilverd, M. A., Rodger, C. J., Gamble, R., Meredith, N. P., Parrot, M., Berthelier, J.-J., & Thomson, N. R. (2008). Ground-based transmitter signals observed from space: Ducted or nonducted? *Journal of Geophysical Research*, 113(A4), A04211. https://doi.org/10.1029/
- Colman, J. J., & Starks, M. J. (2013). Vlf wave intensity in the plasmasphere due to tropospheric lightning. *Journal of Geophysical Research: Space Physics*, 118(7), 4471–4482. https://doi.org/10.1002/jgra.50217
- Edgar, B. C. (1976). The upper- and lower-frequency cutoffs of magnetospherically reflected whistlers. *Journal of Geophysical Research* (1896-1977), 81(1), 205–211. https://doi.org/10.1029/JA081i001p00205
- Fiser, J., Chum, J., Diendorfer, G., Parrot, M., & Santolik, O. (2010). Whistler intensities above thunderstorms. *Annales Geophysicae*, 28(1), 37–46. https://doi.org/10.5194/angeo-28-37-2010
- Gemelos, E. S., Inan, U. S., Walt, M., Parrot, M., & Sauvaud, J. A. (2009). Seasonal dependence of energetic electron precipitation: Evidence for a global role of lightning. *Geophysical Research Letters*, 36(21), L21107. https://doi.org/10.1029/2009GL040396
- Green, A., Li, W., Ma, Q., Shen, X.-C., Bortnik, J., & Hospodarsky, G. B. (2020). Properties of lightning generated whistlers based on van allen probes observations and their global effects on radiation belt electron loss. *Geophysical Research Letters*, 47(17), e2020GL089584. https://doi.org/10.1029/2020GL089584
- Hartley, D. P., Kletzing, C. A., Chen, L., Horne, R. B., & Santolík, O. (2019). Van allen probes observations of chorus wave vector orientations:
 Implications for the chorus-to-hiss mechanism. Geophysical Research Letters, 46(5), 2337–2346. https://doi.org/10.1029/2019GL082111
 Helliwell, R. A. (1965). Whistlers and related ionospheric phenomena/. Stanford University Press.
- Helliwell, R. A. (1969). Low-frequency waves in the magnetosphere. Reviews of Geophysics, 7(1-2), 281-303. https://doi.org/10.1029/RG007i001p00281
- Ho, D., & Bernard, L. (1973). A fast method to determine the nose frequency and minimum group delay of a whistler when the causative spheric is unknown. *Journal of Atmospheric and Terrestrial Physics*, 35(5), 881–887, https://doi.org/10.1016/0021-9169(73)90070-6
- Horne, R. B. (1989). Path-integrated growth of electrostatic waves: The generation of terrestrial myriametric radiation. *Journal of Geophysical Research*, 94(A7), 8895–8909. https://doi.org/10.1029/JA094iA07p08895
- Inan, U. S., & Bell, T. F. (1977). The plasmapause as a vlf wave guide. Journal of Geophysical Research (1896-1977), 82(19), 2819–2827. https://doi.org/10.1029/JA082i019p02819
- Inan, U. S., Piddyachiy, D., Peter, W. B., Sauvaud, J. A., & Parrot, M. (2007). Demeter satellite observations of lightning-induced electron precipitation. *Geophysical Research Letters*, 34(7), L07103. https://doi.org/10.1029/2006GL029238
- Jacobson, A. R., Holzworth, R. H., Pfaff, R. F., & McCarthy, M. P. (2011). Study of oblique whistlers in the low-latitude ionosphere, jointly with the c/nofs satellite and the world-wide lightning location network. *Annales Geophysicae*, 29(5), 851–863. https://doi.org/10.5194/angeo-29-851-2011
- Kletzing, C. A., Kurth, W. S., Acuna, M., MacDowall, R. J., Torbert, R. B., Averkamp, T., et al. (2013). The electric and magnetic field instrument suite and integrated science (EMFISIS) on RBSP. Space Science Reviews, 179(1–4), 127–181. https://doi.org/10.1007/s11214-013-9993-6
- Liu, X., Gu, W., Xia, Z., Chen, L., & Horne, R. B. (2021). Frequency-dependent modulation of whistler-mode waves by density irregularities during the recovery phase of a geomagnetic storm. *Geophysical Research Letters*, 48(16), e2021GL093095. https://doi.org/10.1029/ 2021GL093095
- Marshall, R. A., Sousa, A., Reid, R., Wilson, G., Starks, M., Ramos, D., et al. (2021). The micro-broadband receiver (µbbr) on the very-low-frequency propagation mapper cubesat. Earth and Space Science, 8(11), e2021EA001951. https://doi.org/10.1029/2021EA001951
- Mauk, B. H., Fox, N. J., Kanekal, S. G., Kessel, R. L., Sibeck, D. G., & Ukhorskiy, A. (2013). Science objectives and rationale for the radiation belt storm probes mission. *Space Science Reviews*, 179(1–4), 3–27. https://doi.org/10.1007/s11214-012-9908-y
- Meredith, N. P., Horne, R. B., Glauert, S. A., & Anderson, R. R. (2007). Slot region electron loss timescales due to plasmaspheric hiss and lightning-generated whistlers. *Journal of Geophysical Research*, 112(A8), A08214. https://doi.org/10.1029/2007JA012413
- Miyoshi, Y., Shinohara, I., Takashima, T., Asamura, K., Higashio, N., Mitani, T., et al. (2018). Geospace exploration project erg. Earth Planets and Space, 70(1), 101. https://doi.org/10.1186/s40623-018-0862-0
- Němec, F., Santolík, O., Parrot, M., & Rodger, C. J. (2010). Relationship between median intensities of electromagnetic emissions in the vlf range and lightning activity. *Journal of Geophysical Research*, 115(A8), A08315. https://doi.org/10.1029/2010JA015296
- Oike, Y., Kasahara, Y., & Goto, Y. (2014). Spatial distribution and temporal variations of occurrence frequency of lightning whistlers observed by vlf/wba onboard akebono. *Radio Science*, 49(9), 753–764. https://doi.org/10.1002/2014RS005523
- Peter, W. B., & Inan, U. S. (2005). Electron precipitation events driven by lightning in hurricanes. *Journal of Geophysical Research*, 110(A5), A05305, https://doi.org/10.1029/2004JA010899
- Ripoll, J.-F., Farges, T., Malaspina, D. M., Cunningham, G. S., Hospodarsky, G. B., Kletzing, C. A., & Wygant, J. R. (2021a). Propagation and dispersion of lightning-generated whistlers measured from the van allen probes. *Frontiers in Physics*, 9, 722355. https://doi.org/10.3389/fphy. 2021.722355

XIA ET AL. 11 of 12

- Ripoll, J. F., Farges, T., Malaspina, D. M., Cunningham, G. S., Lay, E. H., Hospodarsky, G. B., et al. (2021b). Electromagnetic power of lightning superbolts from earth to space. *Nature Communications*, 12(1), 3553. https://doi.org/10.1038/s41467-021-23740-6
- Ripoll, J.-F., Farges, T., Malaspina, D. M., Lay, E. H., Cunningham, G. S., Hospodarsky, G. B., et al. (2020). Analysis of electric and magnetic lightning-generated wave amplitudes measured by the van allen probes. *Geophysical Research Letters*, 47(6), e2020GL087503. https://doi.org/10.1029/2020GL087503
- Rodger, C. J., Clilverd, M. A., & McCormick, R. J. (2003). Significance of lightning-generated whistlers to inner radiation belt electron lifetimes. Journal of Geophysical Research, 108(A12), 1462. https://doi.org/10.1029/2003JA009906
- Santolík, O., Parrot, M., Inan, U. S., Burešová, D., Gurnett, D. A., & Chum, J. (2009). Propagation of unducted whistlers from their source lightning: A case study. *Journal of Geophysical Research*, 114(A3), A03212. https://doi.org/10.1029/2008JA013776
- Santolík, O., Parrot, M., & Lefeuvre, F. (2003). Singular value decomposition methods for wave propagation analysis. *Radio Science*, 38(1), 1010. https://doi.org/10.1029/2000RS002523
- Smith, R. L. (1961). Propagation characteristics of whistlers trapped in field-aligned columns of enhanced ionization. *Journal of Geophysical Research* (1896-1977), 66(11), 3699–3707. https://doi.org/10.1029/JZ066i011p03699
- Smith, R. L., Helliwell, R. A., & Yabroff, I. W. (1960). A theory of trapping of whistlers in field-aligned columns of enhanced ionization. *Journal of Geophysical Research* (1896-1977), 65(3), 815–823. https://doi.org/10.1029/JZ065i003p00815
- Starks, M. J., Albert, J. M., Ling, A. G., O'Malley, S., & Quinn, R. A. (2020). Vlf transmitters and lightning-generated whistlers: 1. Modeling waves from source to space. *Journal of Geophysical Research: Space Physics*, 125(3), e2019JA027029. https://doi.org/10.1029/2019JA027029
- Storey, L. R. O. (1953). An investigation of whistling atmospherics. *Philosophical Transactions of the Royal Society of London, Series A*, 246(908), 113–141. https://doi.org/10.1098/rsta.1953.0011
- Streltsov, A. V. (2021a). Whistler on a shelf. Journal of Geophysical Research: Space Physics, 126(5), e2021JA029403. https://doi.org/10.1029/2021JA029403
- Streltsov, A. V. (2021b). Whistlers in the plasmasphere. Journal of Geophysical Research: Space Physics, 126(2), e2020JA028933. https://doi.org/10.1020/2020JA028933
- org/10.1029/2020JA028933
 Streltsov, A. V. (2022). On a guiding of whistler-mode waves by density gradients. *Journal of Geophysical Research: Space Physics*, 127(12),
- e2022JA031056. https://doi.org/10.1029/2022JA031056 Streltsov, A. V., Lampe, M., Manheimer, W., Ganguli, G., & Joyce, G. (2006). Whistler propagation in inhomogeneous plasma. *Journal of*
- Geophysical Research, 111(A3), A03216. https://doi.org/10.1029/2005JA011357

 Tao X. Bortnik J. & Friedrich M. (2010). Variance of transionospheric VI F wave power absorption. Journal of Geophysical Research: Space
- Tao, X., Bortnik, J., & Friedrich, M. (2010). Variance of transionospheric VLF wave power absorption. *Journal of Geophysical Research: Space Physics*, 115(A7), A07303. https://doi.org/10.1029/2009ja015115
- Zheng, H., Holzworth, R. H., Brundell, J. B., Jacobson, A. R., Wygant, J. R., Hospodarsky, G. B., et al. (2016). A statistical study of whistler waves observed by van allen probes (rbsp) and lightning detected by wwlln. *Journal of Geophysical Research: Space Physics*, 121(3), 2067–2079. https://doi.org/10.1002/2015JA022010

XIA ET AL. 12 of 12